

Variance scaling in shallow cumulus topped mixed layers

By R. A. J. Neggers*, B. Stevens and J. D. Neelin

Department of Atmospheric and Oceanic Sciences, University of California at Los Angeles

Submitted to QJRMS September 1, 2006

SUMMARY

Scaling of thermodynamic variance in shallow cumulus topped mixed layers is studied using large-eddy simulation (LES). First the performance of top-down scaling, consisting of the turbulent flux at mixed layer top divided by w^* , is evaluated for transient shallow cumulus convection over land. The results indicate that this top-down scale fails to capture all variance in the top half of the mixed layer when shallow cumulus clouds are present. A variance budget analysis is then performed to derive a new scaling for the variance at mixed layer top, which differs from the standard top-down scale by one Richardson number. The essential new features of the proposed scaling are that i) the local vertical gradient is retained, and ii) a balance is assumed between gradient production of variance on the one hand, and removal by transport and dissipation on the other, using an adjustment time scale given by w_*/h . Evaluation against LES for a range of different shallow cumulus cases, including both steady-state marine and transient continental situations, reveals a data-collapse of the newly scaled variance of all hours and all cases in the top half of the sub-cloud mixed layer. The corresponding vertical structure is shown to resemble a power-law function. In transient situations the scaling reproduces the time-development of variance at sub-cloud mixed layer top. The new cloud base variance scale is then further interpreted in the context of statistical cloud schemes, which rely on the variance as the second moment of the associated probability density function. The result suggests that the area fraction of the moist convective thermals uniquely depends on the ratio of cloud base transition layer depth to sub-cloud mixed layer depth. This puts “valve” or ventilation type closures for the cloud base mass flux in the context of the variance-budget for the sub-cloud layer.

KEYWORDS: Shallow cumulus Variance scaling Transition Layer Mass flux closure

1. INTRODUCTION

The parameterization of vertical transport of heat, humidity and momentum by shallow cumulus cloud populations has been the subject of intensive research (see e.g. Arakawa (2004) for a recent review). The mass flux approach has emerged as one of the more successful methods, in which the vertical advective transport by organized updrafts is explicitly modeled (e.g. Ooyama, 1971; Yanai et al., 1973; Betts, 1975; Siebesma and Cuijpers, 1995). The mass flux is defined as the product of air density, convective area fraction and vertical velocity of the associated updrafts. While most bulk closure methods parameterize the mass flux as a single entity, the area fraction and vertical velocity can also be modelled individually. For instance, updraft vertical velocity can be estimated from the integrated mixed layer buoyancy flux (e.g. Grant, 2001), while the associated convective area fraction can be retained and explicitly parameterized (e.g. Neggers et al., 2004; Bretherton et al., 2004). The area fraction can be estimated using an assumption for the underlying distribution of the thermodynamic state variables (Sommeria and Deardorff, 1977), as constrained by the prediction of one or more moments of that distribution. Even the simplest of these PDF-based approaches requires knowledge of the variance of temperature and humidity. This raises the question motivating this study: what determines the structure of the variance at the top of the sub-cloud mixed layer.

* *Current affiliation:* European Centre for Medium-range Weather Forecasts. *Corresponding author address:* R. A. J. Neggers, ECMWF, Shinfield Park, Reading, Berkshire, RG2 9AX, UK. E-mail: Roel.Neggers@ecmwf.int
© Royal Meteorological Society, 200?.

Standard similarity theory for the convective mixed layer, or mixed layer scaling, grew out of attempts to understand the similarity structure of the surface layer in the early 1970s (see e.g. Stull (1988) for a review). Near the surface in shear free convective layers it is often argued that conserved scalars follow the free-convective temperature scaling of Wyngaard et al. (1971) and Kaimal et al. (1976), wherein the non-dimensional variance of some scalar c scales as

$$\frac{\sigma_c^2}{c_*^2} = \alpha \left(\frac{z}{h} \right)^{-2/3} \quad \text{where} \quad c_* \equiv \frac{\overline{w'c'_0}}{w_*}, \quad (1)$$

The over-line denotes the mean value and the prime denotes fluctuations, so that $c = \bar{c} + c'$. Values at $z = 0$ are denoted by subscript 0, these valid at the top of the sub-cloud mixed layer, $z = h$, are denoted by h . The Deardorff or convective velocity scale is denoted by w_* .

Field measurements from Minnesota reported by Kaimal et al. (1976) show that the potential temperature variance conforms well to (1) in the lower part of the mixed layer ($z < 0.1h$) with the constant of proportionality, $\alpha = 1.8$. However, this scaling works less well above $z > 0.1h$. Between 0.1 and $0.5h$ θ^2 tended to decrease more rapidly than the theory predicted, while θ^2 tended to increase again above $0.5h$. Kaimal et al. (1976) recognized the tendency of θ^2 to increase with z above $0.5h$ to be a signature of entrainment, a process not accounted for in the arguments leading up to (1). Subsequent work by a number of investigators (e.g., Deardorff, 1974b; Nicholls and LeMone, 1980; Lenschow et al., 1980; Caughey, 1982) reinforced these findings, and helped motivate the concept of top-down and bottom up scalar diffusion (Wyngaard and Brost, 1984). According to these ideas, the fundamental asymmetry of the convective forcing of the CBL, wherein the buoyancy flux is positive at the surface and some negative fraction of the surface forcing at the top of the PBL, causes scalars mixing into the PBL from the top (top-down) to diffuse through the PBL differently than scalar fluxes originating at the bottom (bottom-up).

Using these ideas, and noting that any scalar c can be written as a linear composition of its top-down and bottom up components c_t and c_b , Moeng and Wyngaard (1984) showed that the scalar variance through the depth of the dry convective boundary layer could be well represented by superimposing the scalar variance expected for pure top-down and bottom-up scalars:

$$\sigma_c^2 = c_{h*}^2 f_h \left(\frac{z}{h} \right) + 2 c_{h*} c_{s*} f_{hs} \left(\frac{z}{h} \right) + c_{s*}^2 f_s \left(\frac{z}{h} \right). \quad (2)$$

In this expression

$$c_{h*} = \frac{\overline{w'c'_h}}{w_*} \quad \text{and} \quad c_{s*} = \frac{\overline{w'c'_0}}{w_*} \quad (3)$$

are separate scales measuring the relative contributions of the top-down and bottom-up component of the scalar, with $\overline{w'c'_0}$ and $\overline{w'c'_h}$ denoting the turbulent flux at the surface and top of the PBL respectively. The height variation of the component variances are carried by the functions f_h and f_s , which Moeng and Wyngaard (1984) deduced empirically on the basis of existing field data and large-eddy simulations.

We ask how well (2) captures the variance profiles of liquid-water potential temperature, θ_l , and total specific humidity, q_t , in the sub-cloud layer of boundary layers topped by shallow cumulus. To answer this question we use a suite of

simulations drawn from past studies that range from nearly stationary maritime shallow cumulus to highly non-stationary cases of shallow cumulus over land. The non-stationary cases are all tied to the diurnal cycle and allow us to explore several different convective regimes within one simulation. This significantly broadens the parameter space compared to studies of more stationary conditions.

Figure 1 shows hourly variance profiles obtained from large eddy simulation (LES) of the diurnal variation of a fair-weather cumulus case over land (see Section 2 for its description). The variance profiles are normalized by the mixed layer top scale c_{h*}^2 , as defined in (3). Near $z = h$, defined as the height of minimum buoyancy flux, this scale dominates over the contributions by the f_s and f_{hs} terms in (2), i.e. using height dependent scaling given by (3) would not improve the scaling in the upper part of the mixed layer. Although c_{h*}^2 explains more of the variance as compared to c_{s*}^2 , the normalized variance profiles still exhibit considerable spread. This is especially evident during the later hours of the diurnal cycle when convection is more intense; the top scale c_{h*}^2 then underestimates the variance.

These observations motivate further study of the vertical structure of variance in shallow cumulus topped mixed layers. In this paper a new top-down variance scale is presented, which differs from (3) through its incorporation of the local gradient. It is found that this scaling more adequately reproduces the structure, magnitude and time development of mixed layer variance, for stationary as well as transient shallow cumulus cases. The new cloud base variance scale is then further interpreted in the context of statistical cloud schemes, by assuming the form of the probability density functions of humidity and temperature. The result suggests that the area fraction of the moist convective thermals uniquely depends on the ratio of cloud base transition layer depth to sub-cloud mixed layer depth. This result puts the type of mass flux closures that explicitly parameterize this area fraction (also known as “valve” type closures, e.g. Mapes, 2000; Bretherton et al., 2004; Neggers et al., 2004) in the context of the full variance budget.

In Section 2 the LES model will be described, as well as the range of shallow cumulus cases that form the basis of this study. In Section 3 the new scaling will be presented, and is evaluated against the LES in Section 4. In Section 5 the important role of the cloud base transition layer in the new scaling will be explored, implying a new closure formulation for the mass flux area fraction. The implications of the results are discussed in Section 6, and some conclusive remarks can be found in Section 7.

2. LES MODEL AND CASE DESCRIPTIONS

The LES runs are performed using the model of the Royal Netherlands Meteorological Institute (KNMI), as described in detail by Cuijpers and Duynkerke (1993). The results presented in this paper are based on a reanalysis of a suite of simulations established over time, of which many were performed in order to take part in the LES inter-comparison studies organized by working group I of GEWEX (Global Energy and Water Experiment) Cloud System Studies (GCSS, Browning, 1993). The details of the model and the numerical simulations, such as domain size and resolution, differ per cumulus case, as described below.

Four shallow cumulus cases are simulated. Two represent relatively steady marine conditions, the other two more transient continental conditions. The first marine case is based on the Barbados Oceanic and Meteorological Experiment

(BOMEX, Holland and Rasmusson, 1973; Nitta and Esbensen, 1974). The LES case setup is based on an undisturbed period during BOMEX, when the cumulus clouds were capped by a Trade inversion at 800 hPa. Further details are given by Siebesma et al. (2003). The second marine case is based on the Atlantic Trade-wind Experiment (ATEX) (Augstein et al., 1973, 1974). It is characterized by a strong capping Trade-wind inversion. The clouds were shallow cumulus rising into a stratocumulus-like layer just below the inversion. The LES case setup is based on an undisturbed period during BOMEX, when the cumulus clouds were capped by a trade inversion at 800 hPa. Further details are given by Stevens et al. (2001).

The first continental diurnal cycle case is based on measurements taken at the Central Facility of the Southern Great Plain site of the Atmospheric Radiation Measurement (ARM) program (Stokes and Schwartz, 1994). The shallow cumulus cloud layer was observed to slowly grow in depth after onset. The LES case setup is described by Brown et al. (2002). The second continental cumulus case is based on the Small Cumulus Microphysics Study (SCMS, see Knight and Miller, 1998; French et al., 1999; Laird et al., 2000). Some relevant boundary layer measurements and the LES case setup are described by Neggers et al. (2003b). Although similar to the ARM case, it is somewhat more humid, and features a relatively high cloud cover in the LES with a peak value of about 40% shortly after cloud onset. The cloud layer also deepens relatively rapidly compared to the ARM case.

3. VARIANCE BUDGET ANALYSIS

The failure of c_{h^*} to fully capture all variance at mixed layer top in the presence of a shallow cumulus cloud layer suggests that either the sub-cloud layer differs from a dry convective PBL, or the dry convective PBL scaling fails to capture periods when the forcing is more rapidly changing. We argue that successful scaling should reflect the coupling between the cloud and sub-cloud layer, and therefore should have information on i) the cumulus cloud layer, ii) the sub-cloud mixed layer and iii) local stability of the transition layer that is situated in between (e.g. Augstein et al., 1974; Albrecht et al., 1979; Yin and Albrecht, 2000). In revisiting this issue we return to the full prognostic equation for the thermodynamic variance. Following Deardorff (1974a) the variance budget can be written as

$$\frac{\partial \sigma_c^2}{\partial t} = -2\overline{w'c'} \frac{\partial \bar{c}}{\partial z} - \frac{\partial \overline{w'c'c'}}{\partial z} - \epsilon, \quad (4)$$

Here $\overline{w'c'c'}$ is the turbulent flux of variance, and ϵ is the molecular dissipation of variance. We have assumed horizontal homogeneity because it is enforced in LES and it simplifies the analysis.

We limit our analysis to the variance budget at the mixed layer top, because the variances at this height are critical to a determination of cloud fraction. Using LES of a developing clear convective boundary layer, Deardorff (1974b) showed that at the top of the dry CBL the gradient-production term is the only source term, representing dry mixed layer thermals that overshoot into the strong gradient and generate variance accordingly. Production is counteracted by transport and dissipation. Figure 2 illustrates that this structure is similar in shallow cumulus situations. This dissipative behavior of transport in the top of

the mixed layer suggests its parameterization in the form of exponential decay. A further analysis of the vertical structure of variance transport at mixed layer top in LES (see Appendix A) suggests that the dissipation timescale τ associated with variance transport in the top half of the mixed layer is

$$\tau \equiv \frac{h}{w_*}. \quad (5)$$

This timescale is similar to that of the decay of convective turbulence, as found by Nieuwstadt and Brost (1986). As a consequence of this similarity, variance dissipation and transport can be represented by a single term, and the steady-state variance budget (4) becomes

$$-\overline{w'c'}_h \left. \frac{\partial \bar{c}}{\partial z} \right|_h \propto \frac{\sigma_c^2|_h}{\tau}, \quad (6)$$

where subscript h refers to the local value at mixed layer top. In this framework, transport and dissipation thus act together to reduce any variance that is produced and maintained by mixed layer thermals overshooting into the transition layer. Relation (6) suggests a new local scale $c_\#$ for the variance at mixed layer top,

$$c_\#^2 \equiv -\overline{w'c'}_h \left. \frac{\partial \bar{c}}{\partial z} \right|_h \frac{h}{w_*}. \quad (7)$$

The remainder of this paper explores this scaling in more depth.

In previous scaling of shallow cumulus variance (Grant and Brown, 1999; Lenderink and Siebesma, 2000) the timescale of relaxation of variance has been modeled as the ratio of cloud layer depth to a vertical velocity scale that is a function of the convective available potential energy (CAPE) of the cloud layer. This choice may be appropriate in the cloud layer - but becomes problematic in the mixed layer in cases of forced cumulus convection (cumulus humilis), in which the clouds never reach their level of free convection and the velocity scale associated with CAPE is zero or negative. A good example is the period shortly after cloud onset in the transient continental convection. The second important novelty of (7) is that it is only applied *locally* at mixed layer top. As a result, through the vertical gradient $\partial_z \bar{c}$ the small jump of temperature and humidity which is often observed at shallow cumulus cloud base (e.g. Augstein et al., 1974; Albrecht et al., 1979; Yin and Albrecht, 2000) is well represented. The presence of this small but significant gradient in the variance production term makes it potentially important for local variance scaling efforts.

4. LES RESULTS

The new variance scaling (7) is now evaluated using LES. Figures 3 and 4 show hourly averaged variance profiles normalized by $c_\#$ for all shallow cumulus cases described in Section 2. The collapse of the profiles near mixed layer top suggests that the scaling applies best in the height range $0.6 < z/h \leq 1$. This range corresponds to the applicability of damping timescale (5) in formulation (A.3) of variance transport. These results suggest that a typical vertical structure exists in the scaled variance profile in the top half of the mixed layer. To illustrate this the scaled variance profiles of all hours and all cases are plotted in one frame in Fig. 5. The dispersion among cases is small.

In order to fit a power-law function to the scaling region the same data is plotted on logarithmic axes, see Fig. 6, in which a linear relation with slope b implies that the variance depends on the non-dimensional height ratio to the power b (so called similarity of the second kind),

$$\frac{\sigma_c^2}{c_{\#}^2} = 0.9 \left(\frac{z}{h} \right)^{b_c}, \quad (8)$$

where the power for specific humidity $b_q = 4$ and potential temperature $b_\theta = 6$ are different. Both fits are also shown in Fig. 5. The powers are different because humidity and temperature contribute differently to buoyancy. The variance peaks at the level of maximum gradient which is slightly higher than the level of minimum buoyancy flux, as already observed by Deardorff (1974b) for the dry CBL. This is reflected in the constants of proportionality used in (8), which are slightly smaller than one. Close to the surface the new variance scaling fails, because cloud base characteristics become less relevant at levels further away from it. At these levels one expects the surface scales to dominate. This motivates combining the surface and mixed layer top scaling into one relation (e.g. Moeng and Wyngaard, 1984),

$$\sigma_c^2(z) = 1.8 \left(\frac{z}{h} \right)^{-\frac{2}{3}} c_{s*}^2 + 0.9 \left(\frac{z}{h} \right)^{b_c} c_{\#}^2. \quad (9)$$

Figure 7 shows the time-series of the variances at mixed layer top during the transient cumulus cases. The performance of $c_{\#}$ is compared to surface scaling c_{s*} and top-down scaling c_{h*} . The new variance scale $c_{\#}$ is most successful in reproducing the time evolution as seen in LES. The surface scale c_{s*} tends to reach its maximum at a much earlier time than the scales for mixed layer top. Using c_{h*} correctly shifts the maximum towards later times, but is still not sufficient. Both scales without information on the local vertical gradient fail to capture the variance minimum that occurs in the ARM case at the 7th hour.

Figure 8 shows the time-series of the local vertical gradients of humidity and temperature at mixed layer top for the land cases. In the course of the day these gradients change significantly. In general, the mixed layer top experiences destabilization in the first hours and stabilization in the last hours of the diurnal cycle. This reflects the development of the coupling between mixed layer and cloud layer. In this respect the ARM case develops considerably differently during the first hours than the SCMS case, in that the former is much more stable above the mixed layer. During the 7th hour in the ARM case the mixed layer top suddenly destabilizes, which is accompanied by a more rapid deepening of the cloud layer (see Fig. 9b). This sudden weakening of the gradients is accompanied by a significant decrease in variance (see Fig. 7c). This suggests that knowledge of the local vertical gradient may be essential in any parameterization of variance.

5. MASS FLUX AREA FRACTION

The results illustrate that the structure of the cloud base transition layer affects the local variance significantly. This interface layer is now studied in more detail, to the purpose of parameterizing its properties that appear in the new variance scaling (7). This is necessary for the broad class of models which do not provide this information naturally and may provide more insight in the important role of the cloud base transition layer in shallow cumulus convection.

Figure 9 shows the typical vertical structure of a shallow cumulus topped boundary layer. Cloud base height z_b is defined as the height of maximum cloud core fraction, defined as the area fraction of positively buoyant clouds (also referred to as the “moist convective thermals”). In prototype shallow cumulus convection the cloud core does most of the vertical transport (Siebesma and Cuijpers, 1995), which justifies its use in the bulk mass flux approach, as subsequently done here. Similar to Grant (2001), the layer of depth Δh between h and z_b is defined as the transition layer. Lenderink and Siebesma (2000) first applied the mass flux approach in the variance production term. Applying this approach, in combination with the use of a bulk gradient approach over the transition layer depth, gives for (7)

$$c_{\#}^2 = M \frac{\Delta c^2}{\Delta h} \frac{h}{w_*}, \quad (10)$$

where M is the cloud base mass flux, and Δc is the jump in the mean vertical profile \bar{c} over the transition layer. Here the humidity excess of the moist convective thermals over the dry environment has been assumed to be proportional to Δc . Figure 10 shows that this assumption is supported by LES. This proportionality is due to the moist convective thermals still carrying properties of the mixed layer where they originate. Their collective volumetric mass flux M is defined as the product of their area fraction \mathcal{A} and their vertical velocity, which at cloud base scales well with w_* (Neggers et al., 2004). This eliminates w_* in (10), yielding

$$c_{\#}^2 \approx \mathcal{A} \Delta c^2 \frac{h}{\Delta h}. \quad (11)$$

Retaining the convective area fraction in the mass flux (e.g. Neggers et al., 2004, 2006) thus makes it appear in the cloud base variance scale. This is intriguing from the perspective of statistical parameterization of area fractions (Sommeria and Deardorff, 1977), which itself relies on the variance as the second moment of the turbulent distribution of humidity and temperature. As a consequence, there are two equations for two unknowns \mathcal{A} and σ_c , thus defining \mathcal{A} and σ_c implicitly. In other words, scaling σ_c with $c_{\#}$ would yield a parameterization for \mathcal{A} .

This implicit representation of \mathcal{A} still requires the definition of the shape-function of the associated turbulent distribution. One could use a Normal distribution (e.g. Sommeria and Deardorff, 1977; Bougeault, 1982). However, these functions have infinite boundaries, while perhaps more appropriate in this problem is the use of a bounded distribution: for example, the most extreme q_t value at cloud base that can theoretically occur, i.e. that of an undiluted updraft, can never exceed its value at its starting height in the mixed layer. Because it has compact support we choose the Beta function (e.g. Tompkins, 2002),

$$B(p, r) = \int_0^1 x^{p-1} (1-x)^{r-1} dx, \quad (12)$$

where p and r are the shape parameters of the distribution. The standard deviation of the Beta function is related to the distribution boundaries a and b as

$$\sigma \equiv \frac{b-a}{p+r} \sqrt{\frac{p r}{p+r+1}}. \quad (13)$$

Figure 11 supports a choice for the boundaries as

$$b - a = 2\Delta c. \quad (14)$$

Assuming an non-skewed distribution ($p = r$) then gives for (13)

$$\frac{\sigma_c^2}{\Delta c^2} = \frac{1}{2p + 1}. \quad (15)$$

The variance is thus related to the local jump in \bar{c} through the shape function of the associated PDF. Substituting this ratio into the cloud base variance scale (11) finally gives

$$\mathcal{A} = \left(\frac{\Delta h}{h} \right) \frac{1}{2p + 1}. \quad (16)$$

This relation states that the area fraction of the cloudy, buoyant thermals is uniquely dependent on the ratio of transition layer depth to sub-cloud mixed layer depth, times a term dependent on the shape of the distribution.

The validity of relation (16) is verified by comparing the ratio M/w_* at z_b to the depth ratio $\Delta h/h$ for all cumulus cases, see Figure 12a. Apparently, the assumption by Grant (2001) of a constant ratio $\Delta h/h$ does not hold for this set of cases, but is found here instead to cover a broad range (0 – 0.3). Despite some scatter the existence of a relation between \mathcal{A} and $\Delta h/h$ is supported by the LES results. The apparent linearity of the LES data suggests that p is constant, implying that the shape of the PDF at cloud base is more or less case-independent. Fitting relation (16) to the LES data results in

$$p \approx 2.2. \quad (17)$$

The side-panels in Fig.11 illustrate that this Beta function indeed resembles the LES distributions reasonably well. Some scatter in Fig.12a can be attributed to the low vertical resolution of these LES runs, which at 40m was of the order of magnitude of Δh . This causes deviations on the x-axis of up to 40m/800m=0.05 (using a typical value for h). Additional simulations at higher vertical resolution and using a shorter averaging timescale could help clarify this issue.

In deriving (16) the numerator Δc of the local vertical gradient has dropped out against σ_c but the denominator Δh is preserved, introducing a coupling between the area fraction of the moist convective thermals and the depth of the transition layer. For example, in situations of strong transition layer stability (large gradients, or small Δh) \mathcal{A} is small, corresponding to a reduced mass flux. The transition layer thus acts as a “valve” in cumulus transport. On the other hand, through the dissipation timescale the mixed layer depth has entered the equation. As a result, deepening sub-cloud mixed layers imply decreasing convective area fractions, a characteristic feature of diurnal cycles of shallow cumulus that is indeed often observed in nature (e.g. Plank, 1969; Neggers et al., 2004) and in LES (e.g. Brown et al., 2002; Neggers et al., 2003a)

6. DISCUSSION

(a) Comparison to Moeng and Wyngaard (1984)

We now return to the Moeng and Wyngaard (1984) scale c_{h*} as discussed in the introduction, and ask the question why and how the new variance scale $c_{\#}$ is

different. Comparing (3) to (7) shows that the two scales are only the same if

$$\overline{w'c'}_h \approx -h w_* \left. \frac{\partial \bar{c}}{\partial z} \right|_h. \quad (18)$$

Figure 13a shows the two sides of (18), confirming that i) they are indeed not the same, and that ii) the vertical gradient (plotted in Fig. 13b) is causing the difference in time development between the scales. Further breakup of the gradient in Fig. 13c and Fig. 13d reveals that growth of the transition layer depth Δh is uniquely responsible for the sudden decrease in the gradient at $t = 7h$, counteracting a strengthening of the jump Δc in the process.

To further illustrate that c_{h*} and $c_{\#}$ are indeed different theoretically and do not revert to each other in some limit, we now apply the bulk gradient approach over the transition layer depth (see Fig.13b),

$$\left. \frac{\partial \bar{c}}{\partial z} \right|_h \approx \frac{\Delta c}{\Delta h}, \quad (19)$$

and the flux entrainment relation at h ,

$$\overline{w'c'}_h = -E \Delta c = -\frac{A}{Ri_h} w_* \Delta c, \quad (20)$$

where E is top-entrainment velocity, A is a constant of proportionality, and

$$Ri_h \equiv \frac{\frac{g}{\theta_0} \Delta \theta_v h}{w_*^2} \quad (21)$$

is the standard bulk Richardson number, with $g\Delta\theta_v/\theta_0$ the buoyancy jump associated with the transition layer. Substitution of (19)-(20) in assumption (18) would give

$$\frac{\Delta h}{h} \propto \frac{Ri_h}{A}. \quad (22)$$

However, Δh is constrained energetically by an interfacial Richardson number, i.e. as the distance that dry plumes whose energy scales with w_*^2 can penetrate into the stable transition layer,

$$\frac{g}{\theta_0} \Delta \theta_v \Delta h = B w_*^2, \quad (23)$$

with B another constant of proportionality. After rewriting this gives

$$\frac{\Delta h}{h} \propto \frac{B}{Ri_h}. \quad (24)$$

Clearly (22) and (24) can not both be true, which again shows that assumption (18) does not hold. Finally substituting (20) in (3) and (19)-(20),(24) in (7) then illustrates that the new local scale $c_{\#}$ is indeed theoretically different from the Moeng and Wyngaard (1984) scale c_{h*} by one Richardson number,

$$c_{\#} \propto Ri_h c_{h*}. \quad (25)$$

(b) *Equilibrium arguments*

Relation (24), as suggested by the dry interface energy budget, states that the ratio $\Delta h/h$ is not constant (as already shown in Fig. 12a) but is proportional to Ri_h^{-1} . The inverse Richardson number also appears in the entrainment rate closure (20) as its factor of proportionality to w_* . This dependence on Ri^{-1} shared by the w^* -proportionality factors in both top entrainment and mass flux can perhaps be better understood from considering the sub-cloud mixed layer mass budget (Stevens, 2006; Neggers et al., 2006),

$$\frac{\partial h}{\partial t} = E - M + w_{\text{LS}}. \quad (26)$$

where w_{LS} is the large scale subsidence rate at h . The mass flux acts as a loss term, while entrainment always acts to increase mixed layer mass. In equilibrium, for simplicity assuming $-w_{\text{LS}} \ll E$, this implies that $M \approx E$. As both mass flux and entrainment rate are proportional to w_* , this means that in equilibrium their associated factors of proportionality have to be equal, which results in the *cumulus equilibrium constraint*

$$\mathcal{A} = \frac{A}{Ri_h}. \quad (27)$$

The dependence of \mathcal{A} on $\Delta h/h$ as implied by the local variance scale $c_{\#}$ in (16) then means that during the equilibration process Δh and h will adjust to such values that constraint (27) is met. Using typical values of $A = 0.2$ and $Ri_h = 60$ (e.g. Stevens, 2006) illustrates that the equilibrium value of \mathcal{A} typically has to be of the order of a few percent only, explaining the small convective cloud fractions that are characteristic of shallow cumulus convection.

(c) *Transient convection*

In transient situations that have not (yet) reached equilibrium $M \neq E$, which means that \mathcal{A} can then deviate from constraint (27). If the equilibrium state is stable, as typically observed in natural cumulus convection, negative feedback mechanisms should exist that act to bring \mathcal{A} towards A/Ri_h , thus equilibrating the system. Several different theories have been proposed in the literature for the mechanism behind the equilibration. Bretherton et al. (2004) related the mass flux efficiency factor to local stability, while alternatively Neggers et al. (2004, 2006) related it to the fraction of rising thermals that condensate at h , through the normalized saturation deficit. Both options have been shown to introduce a negative feedback mechanism in the mass flux that acts to equilibrate the system.

We now use results of this study to argue that these two methods are in fact different descriptions of the same physical process, by showing that transition layer stability, its depth and the moist convective area fraction are related quantities. The spread of total specific humidity values over the updraft PDF implies that their lifting condensation levels will be at different heights, due to the decrease of saturation specific humidity q_s with height. The depth of the layer Δh in which all updraft LCLs are situated can thus be expressed in terms of the fraction \mathcal{A} of the turbulent PDF that represents those updrafts,

$$\Delta h \frac{\partial q_s}{\partial z} = \mathcal{F}(\mathcal{A}) \sigma_{q_t} \quad (28)$$

where $\mathcal{F}(\mathcal{A})$ is a function dependent on the shape of the PDF, and where for simplicity we excluded the small impact of temperature variations within the PDF on q_s from the argument. The condensate produced by the updraft with the lowest LCL as it rises through that layer is associated with a buoyancy increase due to latent heating,

$$\Delta\theta_v = \frac{L}{c_p} \Delta q_l = \frac{L}{c_p} \Delta h \frac{\partial q_s}{\partial z} \quad (29)$$

Accordingly, when a larger fraction of rising updrafts reaches its LCL, for example as a result of destabilization above mixed layer top, this has to correspond to a deeper transition layer, in which the fraction of updrafts is also more buoyant. The existence of this relation between moist convective area fraction, transition layer depth and updraft buoyancy is supported by LES, see Fig. 12a and b.

The results underline the important role played by the vertical gradient of the saturation specific humidity in the equilibration of the shallow convective PBL. Through (28) it affects the area fraction (or efficiency) of cumulus mass transport, constituting a negative feedback mechanism which ensures that the mean thermodynamic state at mixed layer top is always kept at a certain close proximity to saturation. In that sense, moist convective transport at mixed-layer top can be said to be 'slaved' to the moist thermodynamic relations.

7. CONCLUSIVE REMARKS

A new local scale $c_{\#}$ for the variance at mixed layer top is introduced, as defined by (7), with the aim of addressing shortcomings of the standard top-down scaling for the dry CBL in situations when shallow cumulus clouds are present. The novelty of this scale $c_{\#}$ is that, in addition to the entrainment flux, information on local (transition layer) stability and the convective mixed layer turnover timescale are incorporated. This significantly improves the scaling of variance in transient cumulus situations. The local vertical gradient changes considerably during the first hours after cloud onset, and affects the local variance through the flux-gradient production term. The data collapse for a range of different LES shallow cumulus cases supports the generality of the scaling.

Through the definition of variance as the second moment of a turbulent distribution, the physics in the variance budget are shown to imply a relation between the mass flux area fraction and the ratio of transition layer depth to mixed layer depth. The numerator, transition layer depth, is shown to represent the negative feedback mechanism between cloud base mass flux, local stability and proximity to saturation at mixed layer top, as described by Bretherton et al. (2004) and Neggers et al. (2006). The denominator, mixed layer depth h , in general increases during diurnal cycles, thus reducing \mathcal{A} . This inverse relation is consistent with observations in nature (Plank, 1969; Joseph and Cahalan, 1990) and LES (Neggers et al., 2003a). An accompanying study by Neggers et al. (2006) explores these feedbacks in more detail by applying this variance scale in a simple bulk equilibrium model for the shallow cumulus topped mixed layer.

The variance scale $c_{\#}$ and the related closure for the mass flux area fraction \mathcal{A} can be of potential use in single column modelling. First, retaining and explicitly modelling the area fraction in the mass flux would introduce an extra degree of freedom in the mass flux closure. This flexibility theoretically allows for gradual transitions between dry and moist convection, by enabling a gradual

onset and time-development of the area fraction of moist convective thermals, as opposed to a sudden introduction or “triggering”. Second, using the area fraction \mathcal{A} as implied by the local variance scale $c_{\#}$ couples the resulting mass flux M to the diagnostic variance budget. In combination with a statistical framework for cloudiness (e.g. Sommeria and Deardorff, 1977; Lewellen and Yoh, 1993) this would make the representation of convective transport and cloudiness fully consistent throughout the model, as both are then based on the same reconstructed turbulent distribution. In a forthcoming study (*“A dual mass flux model for boundary layer convection”, in preparation for J. Atmos. Sci.*) these concepts are explored using the single column model of the Integrated Forecasting System (IFS) of the European Centre for Medium-range Weather Forecasts (ECMWF).

The LES cases used for evaluation in this study are of very different nature, featuring both steady state marine and transient continental cases, with surface Bowen ratios ranging from ≈ 0.03 to 0.3. Nevertheless, different scenarios can still be thought of for which it is yet unknown if the scaling still applies. For example, studying cases with strong vertical wind-shear is interesting, as mechanical turbulence might represent a significant source in the variance budget. Evaluation of the validity of the variance scaling against observations remains future work.

Studying the variance structure in transient shallow cumulus cases such as the ARM and SCMS has the benefit that we get an understanding of their behavior for more complex scenarios than steady state situations. This significantly expands the parameter range that is covered. The time-dependency of the variance introduces challenges for parameterization. The closures as presented here have directly been inspired by the study of these diurnal cycle cases. This emphasizes the importance of setting up as many different cases as possible, preferably based on reliable observational data. The research efforts such as by GCSS boundary layer working group I to extract cases from observations have directly contributed to the wealth of moist-convective cases that are now available to the boundary layer modelling community.

ACKNOWLEDGEMENTS

This research was supported in part by National Science Foundation grants DMS-0139666 and ATM-0082529, and National Oceanographic and Atmospheric Administration grant NA05OAR4311134. The LES results in this study were obtained using the model of the Royal Netherlands Meteorological Institute (KNMI), using the supercomputer facilities of the ECMWF in Reading, UK. The LES runs were performed by the first author when affiliated at KNMI, at that time being supported by the European Project for Cloud Systems Studies (EUROCS) as well as the Netherlands Organization for Scientific Research (NWO) under Grant 750.198.06.

APPENDIX A

Variance transport

A decomposition is made of the vertical variance flux into contributions by strong updrafts and their environment,

$$\overline{w'q'q'} = a^{up}\overline{w'q'q'}^{up} + (1 - a^{up})\overline{w'q'q'}^{en}, \quad (\text{A.1})$$

where the superscript *up* represents the average over the updrafts, and *en* represents everything else. The updraft area fraction a^{up} represents a fixed top-percentage of the tail of the PDF of vertical velocity, here chosen to be 5%. The dashed line in Fig. 14 shows that variance transport is dominated by the strongest updrafts, so that the environmental contribution can be neglected. The figure also shows the so-called “top-hat” approximation for the updraft fraction, i.e. neglecting sub-ensemble internal variability. This still captures the bulk of the total transport. This suggests that

$$\frac{\overline{\partial w'q'q'}^{up}}{\partial z} \approx \frac{\partial w^{up}\sigma_q^2}{\partial z} \approx w_* \frac{\partial \sigma_q^2}{\partial z} \quad (\text{A.2})$$

where the last approximation is justified by the smallness of the deceleration term $\sigma_q^2 \frac{\partial w^{up}}{\partial z}$, see Fig. 14. Accordingly, only the term representing vertical advection of variance by the strong updrafts is retained, their vertical velocity w^{up} being assumed to scale with w_* . Then applying the bulk gradient approach over the top half of the mixed layer results in

$$w_* \frac{\Delta \sigma_q^2}{\Delta z} \propto \frac{\sigma_q|_h^2}{\tau}, \quad (\text{A.3})$$

where timescale $\tau \sim h/w_*$ is the adjustment timescale that can be used to describe the effect of organized transport on the variance in the top of the sub-cloud mixed layer. Use is made of the typical vertical structure of variance over the top half of the mixed layer ($\Delta z = \frac{1}{2}h$), with magnitudes in the middle typically about an order of magnitude smaller than at the top (see Fig.3-4). This method thus conforms to an upwind approach for vertical advection. At other heights variance transport behaves differently, and accordingly this timescale is not applicable there.

REFERENCES

- | | | |
|---|------|---|
| Albrecht, B. A., A. K. Betts, W. H. Schubert and S. K. Cox | 1979 | A model of the thermodynamic structure of the Trade-wind boundary layer. Part I: Theoretical formulation and sensitivity tests. <i>J. Atmos. Sci.</i> , 36 , 73-89. |
| Arakawa, A. | 2004 | The cumulus parameterization problem: past, present, and future. <i>J. Clim.</i> , 17 , 2493-2525. |
| Augstein, E., H. Riehl, F. Ostapoff and V. Wagner | 1973 | Mass and energy transports in an undisturbed Atlantic trade-wind flow. <i>Mon. Wea. Rev.</i> , 101 , 101-111. |
| Augstein, E., H. Schmidt and V. Wagner | 1974 | The vertical structure of the atmospheric planetary boundary layer in undisturbed Trade winds over the Atlantic Ocean. <i>Bound.-Layer Meteor.</i> , 6 , 129-150. |
| Betts, A. K. | 1975 | Parametric interpretation of Trade-wind cumulus budget studies. <i>J. Atmos. Sci.</i> , 32 , 1934-1945. |
| Bougeault, P. | 1982 | Cloud ensemble relations based on the Gamma probability distribution for the high-order models of the planetary boundary layer. <i>J. Atmos. Sci.</i> , 39 , 2691-2700. |
| Bretherton, C. S., J. R. McCaa and H. Grenier | 2004 | A new parameterization for shallow cumulus convection and its application to marine subtropical cloud-topped boundary layers. Part I: Description and 1D results. <i>Mon. Wea. Rev.</i> , 132 , 864-882. |
| Brown, A. R., A. Chlond, C. Golaz, M. Khairoutdinov, D. C. Lewellen, A. P. Lock, M. K. MacVean, C-H. Moeng, R. A. J. Neggers, A. P. Siebesma and B. Stevens | 2002 | Large-eddy simulation of the diurnal cycle of shallow cumulus convection over land. <i>Quart. J. Roy. Met. Soc.</i> , 128 , 1075-1094. |

- Browning, K. A. 1993 The GEWEX Cloud System Study (GCSS). *Bull. Amer. Meteor. Soc.*, **74**, 387-399.
- Caughey, S. J. 1982 Observed characteristics of the atmospheric boundary layer. *Atmospheric Turbulence and Air Pollution Modelling*, F. T. M. Nieuwstadt and H. van Dop, Eds. D. Reidel, 107-158.
- Cuijpers, J. W. M., and P. G. Duynkerke 1993 Large-eddy simulation of trade-wind cumulus clouds. *J. Atmos. Sci.*, **50**, 3894-3908.
- Deardorff, J. W. 1974a Three-dimensional numerical study of the height and mean structure of a heated planetary boundary layer. *Bound.-Layer Meteor.*, **7**, 81-106.
- Deardorff, J. W. 1974b Three-dimensional numerical study of turbulence in an entraining mixed layer. *Bound.-Layer Meteor.*, **7**, 199-226.
- French, J. R., G. Vali and R. D. Kelly 1999 Evolution of small cumulus clouds in Florida: observations of pulsating growth. *Atmospheric Research*, **52**, 143-165.
- Grant, A. L. M., and A. R. Brown 1999 A similarity hypothesis for shallow-cumulus transports. *Quart. J. Roy. Met. Soc.*, **125**, 1913-1936.
- Grant, A. L. M. 2001 Cloud-base fluxes in the cumulus-capped boundary layer. *Quart. J. Roy. Met. Soc.*, **127**, 407-421.
- Grant, A. L. M., and A. P. Lock 2004 The turbulent kinetic energy budget for shallow cumulus convection. *Quart. J. Roy. Met. Soc.*, **130**, 401-422.
- Holland, J. Z., and E. M. Rasmusson 1973 Measurement of atmospheric mass, energy and momentum budgets over a 500-kilometer square of tropical ocean. *Mon. Wea. Rev.*, **101**, 44-55.
- Joseph, J. H., and R. F. Cahalan 1990 Nearest neighbor spacing of fair weather cumulus clouds. *J. App. Met.*, **29**, 793-805.
- Kaimal, J. C., J. C. Wyngaard, D. A. Haugen, O. R. Coté and Y. Izumi 1976 Turbulence structure in the convective boundary layer *J. Atmos. Sci.* **33**, 2152-2169
- Knight, C. A. and L. J. Miller 1998 Early radar echoes from small, warm cumulus: Bragg and hydrometeor scattering. *J. Atmos. Sci.*, **55**, 2974-2992.
- Laird, N. F., H. T. Ochs III, T. M. Rauber and L. J. Miller 2000 Initial precipitation formation in warm Florida cumulus. *J. Atmos. Sci.*, **57**, 3740-3751.
- Lenderink, G., and A. P. Siebesma 2000 Combining the massflux approach with a statistical cloud scheme. *Proceedings of the 14th AMS conference on Boundary Layers and Turbulence, Aspen, CO, July 2000*.
- Lenschow, D. H., J. C. Wyngaard and W. T. Pennell 1980 Mean-field and second-moment budgets in a baroclinic, convective boundary layer. *J. Atmos. Sci.*, **37**, 1313-1326.
- Lewellen, W. S., and S. Yoh 1993 Binormal model of ensemble partial cloudiness. *J. Atmos. Sci.*, **50**, 1228-1237.
- Mapes, B. E. 2000 Convective inhibition, subgrid-scale triggering energy, and stratiform instability in a toy tropical wave model. *J. Atmos. Sci.*, **57**, 1515-1535.
- Moeng, Chin-Hoh and John C. Wyngaard 1984 Statistics of conservative scalars in the convective boundary layer, *J. Atmos. Sci.*, **41**, 3161-3169.
- Neggers, R. A. J., H. J. J. Jonker and A. P. Siebesma 2003a Size statistics of cumulus cloud populations in large-eddy simulations. *J. Atmos. Sci.*, **60**, 1060-1074.
- Neggers, R. A. J., P. G. Duynkerke and S. M. A. Rodts 2003b Shallow cumulus convection: A validation of large-eddy simulation against aircraft and Landsat observations. *Q. J. Roy. Met. Soc.*, **129**, 2671-2696.
- Neggers, R. A. J., A. P. Siebesma, G. Lenderink and A. A. M. Holtslag 2004 An evaluation of mass flux closures for diurnal cycles of shallow cumulus. *Mon. Wea. Rev.*, **132**, 2525-2538.
- Neggers, R. A. J., B. Stevens and J. D. Neelin 2006 A simple equilibrium model for shallow cumulus topped mixed layers. *Theoret. Comput. Fluid Dynamics, in press, September 2006*.
- Nicholls, S., and M. A. LeMone 1980 The fair weather boundary layer in GATE: the relationship of subcloud fluxes and structure to the distribution and enhancement of cumulus clouds. *J. Atmos. Sci.*, **37**, 2051-2067.
- Nieuwstadt, F. T. M., and R. A. Brost 1986 The decay of convective turbulence. *J. Atmos. Sci.*, **43**, 532-546.
- Nitta, T. and S. Esbensen 1974 Heat and moisture budget analyses using BOMEX data. *Mon. Wea. Rev.*, **102**, 17-28.

- Ooyama, K. 1971 A theory on parameterization of cumulus convection. *J. Meteor. Soc. Japan*, **49**, 744-756.
- Plank, V. G. 1969 The size distributions of cumulus clouds in representative Florida populations. *J. App. Met.*, **8**, 46-67.
- Siebesma, A. P., and J. W. M. Cuijpers 1995 Evaluation of parametric assumptions for shallow cumulus convection. *J. Atmos. Sci.*, **52**, 650-666.
- Siebesma, A. P., C. S. Bretherton, A. Brown, A. Chlond, J. Cuxart, P. G. Duynkerke, H. Jiang, M. Khairoutdinov, D. Lewellen, C.-H. Moeng, E. Sanchez, B. Stevens, and D. E. Stevens 2003 A large eddy simulation intercomparison study of shallow cumulus convection. *J. Atmos. Sci.*, **60**, 1201-1219.
- Sommeria, G., and J. W. Deardorff 1977 Subgrid-scale condensation in models of non-precipitating clouds. *J. Atmos. Sci.*, **34**, 344-355.
- Stevens, B., A. S. Ackerman, B. A. Albrecht, A. R. Brown, A. Chlond, J. Cuxart, P. G. Duynkerke, D. C. Lewellen, M. K. MacVean, R. A. J. Neggers, E. Sanchez, A. P. Siebsema, D. E. Stevens 2001 Simulations of Trade-wind cumuli under a strong inversion. *J. Atmos. Sci.*, **58**, 1870-1891.
- Stevens, B. 2006 Boundary layer concepts for simplified models of tropical dynamics. *Theoret. Comput. Fluid Dynamics, in press, September 2006*.
- Stokes, G. M., and S. E. Schwartz 1994 The Atmospheric Radiation Measurement (ARM) program: programmatic background and design of the cloud and radiation test bed. *Bull. Amer. Meteor. Soc.*, **75**, 1201-1222.
- Stull, R. B. 1988 *An introduction to boundary layer meteorology*. Kluwer Academic Publishers, 666pp.
- Tompkins, A. 2002 A prognostic parameterization for the subgrid-scale variability of water vapor and clouds in large-scale models and its use to diagnose cloud cover. *J. Atmos. Sci.*, **59**, 1917-1942.
- Yanai, M., S. Esbensen and J.-H. Chu 1973 Determination of bulk properties of tropical cloud clusters from large-scale heat and moisture budgets. *J. Atmos. Sci.*, **30**, 611-627.
- Yin, B., and B. A. Albrecht 2000 Spatial variability of atmospheric boundary layer structure over the eastern equatorial Pacific. *J. Clim.*, **13**, 1574-1592.
- Wyngaard, J. C., O. R. Cote, and Y. Izumi 1971 Local free convection, similarity, and the budgets of shear stress and heat flux. *J. Atmos. Sci.*, **28**, 1171-1182.
- Wyngaard, J. C., and R. A. Brost 1984 Top-down and bottom-up diffusion of a scalar in the convective boundary layer. *J. Atmos. Sci.*, **41**, 102-112.

REFERENCES

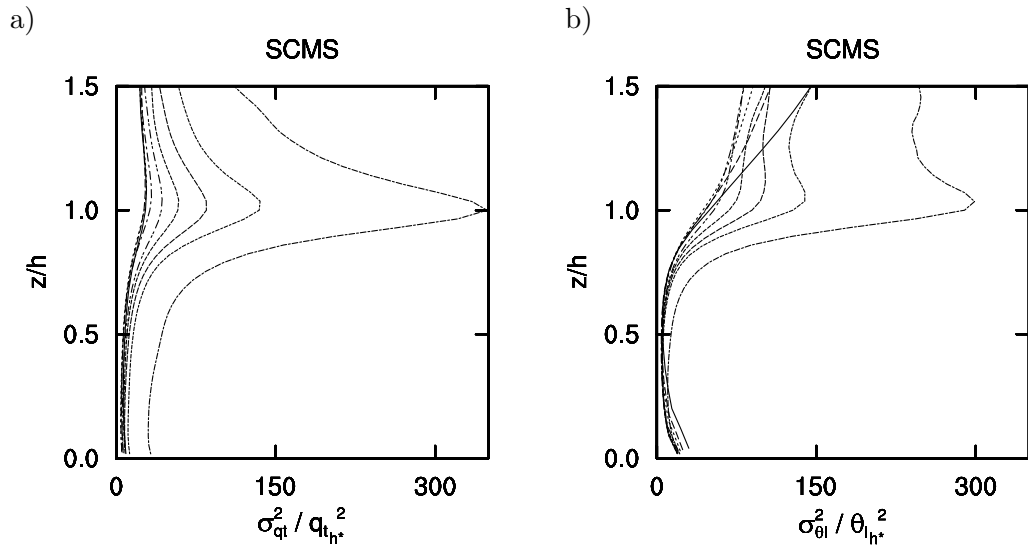


Figure 1. Scaled hourly-mean vertical profiles of the variance of a) total specific humidity q_t and b) liquid water potential temperature θ_l during the continental cumulus case based on the Small Cumulus Microphysics Study (SCMS). The height is scaled by mixed layer height h , defined as the height of minimum buoyancy flux, and the variance is normalized by the mixed layer top scale $c_{h^*}^2$, as defined in (3).

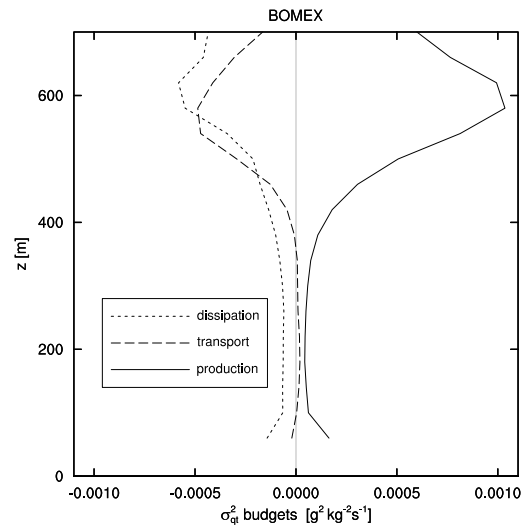


Figure 2. The steady-state humidity variance budget equation (4) for the BOMEX case, as sampled in LES. Production and transport are calculated, and dissipation is obtained as their residual. Cloud base in BOMEX is at about 600m

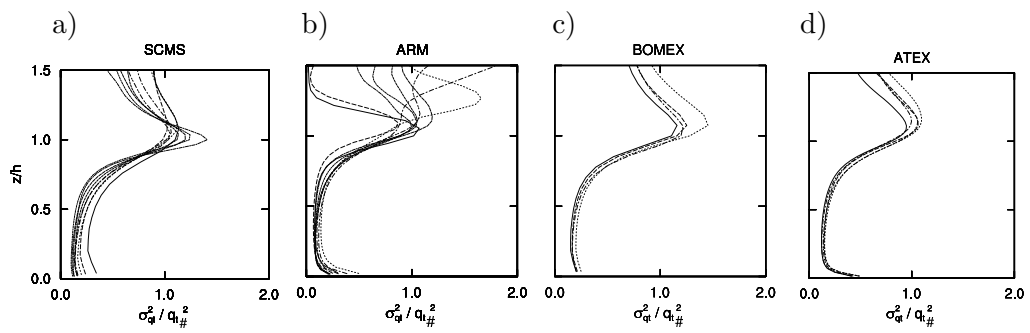


Figure 3. Vertical profiles of the moisture variance for all cases. The height is scaled with mixed layer depth h , and the variance is normalized by the new scale $c_{\#}^2$.

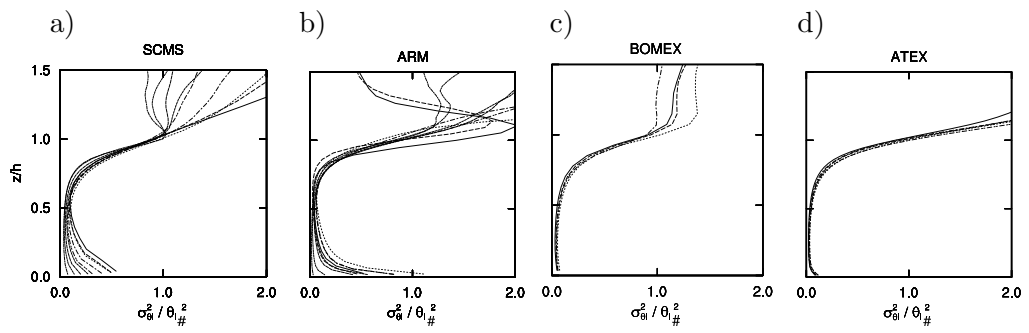


Figure 4. Same as Fig. 3 but now for the liquid water potential temperature.

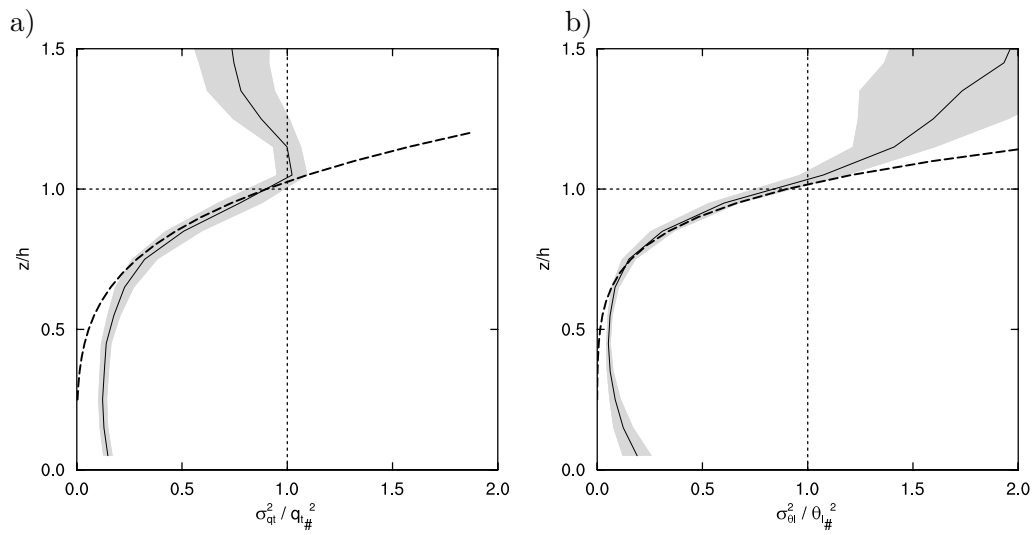


Figure 5. Same as Figures 3 and 4, but now including all cases and all hours. The black solid line is the mean, while the grey area indicates the standard deviation. The thick dashed lines represent the power-law fits (8).

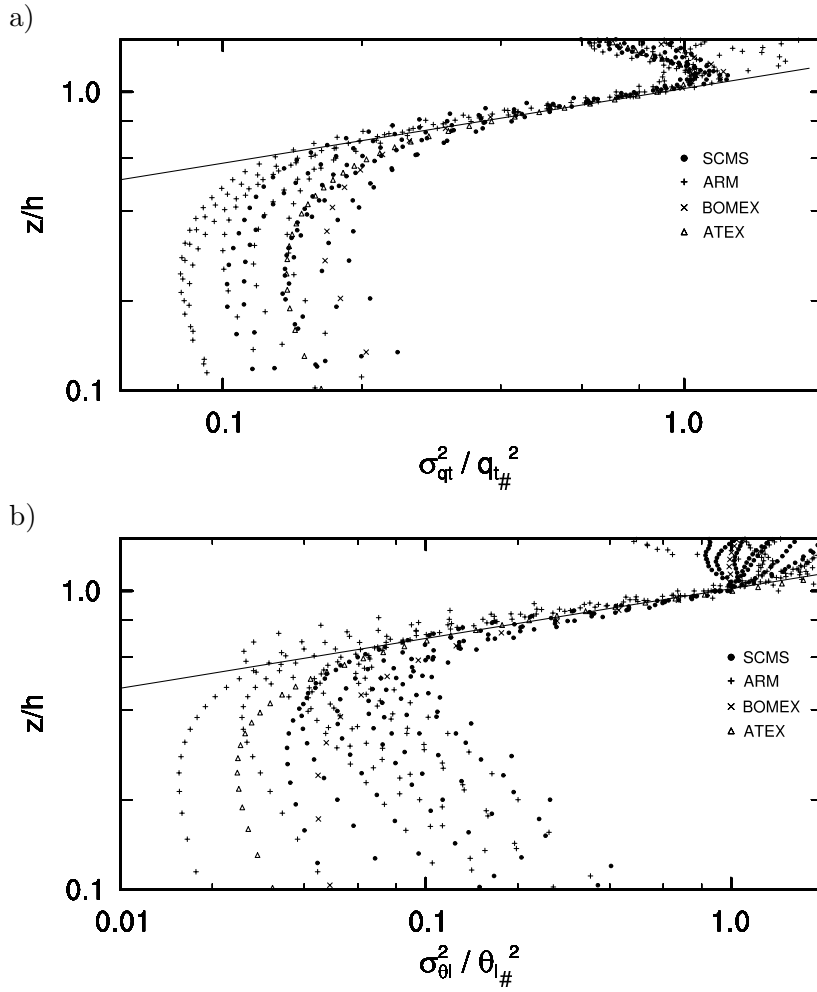


Figure 6. Logarithmic scatter plot of the scaled variance profiles of all cases and all hours. The black solid line represents a power-law fit through the upper part of the sub-cloud layer that shows evidence of scaling behavior. The slope of the fit corresponds to the power, which is 4 for specific humidity and 6 for potential temperature, see (8).

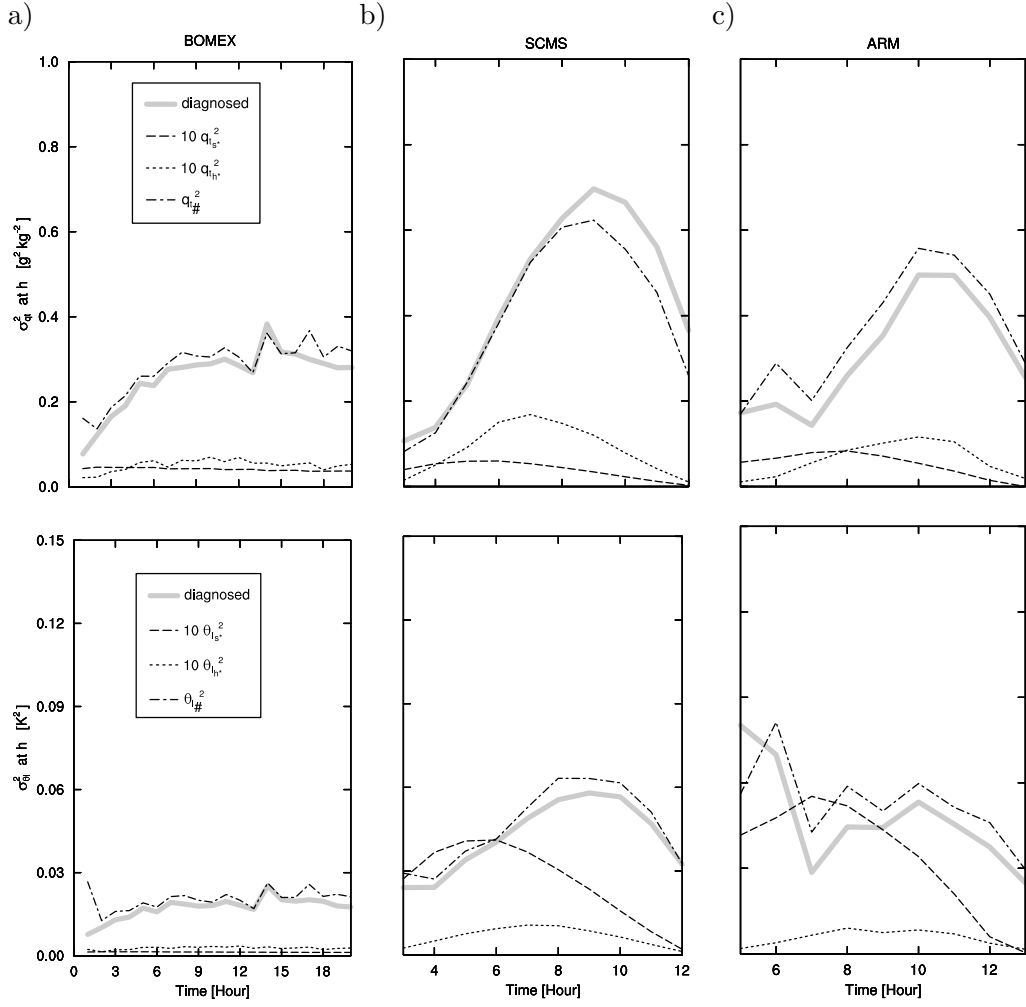


Figure 7. Time-series of the diagnosed variances of q_t and θ_l at mixed-layer top (grey), as well as the corresponding variance scales c_{s*} , c_{l*} and $c_{\#}$ (black), during a) BOMEX, b) SCMS and c) ARM. Some scales are multiplied by a factor 10 for purpose of display.

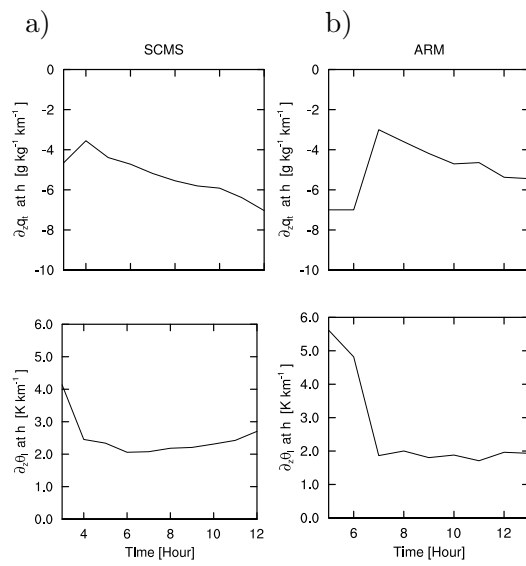


Figure 8. Time-series of the local vertical gradients of total specific humidity and liquid water potential temperature at mixed layer top h during the a) SCMS case and b) ARM case.

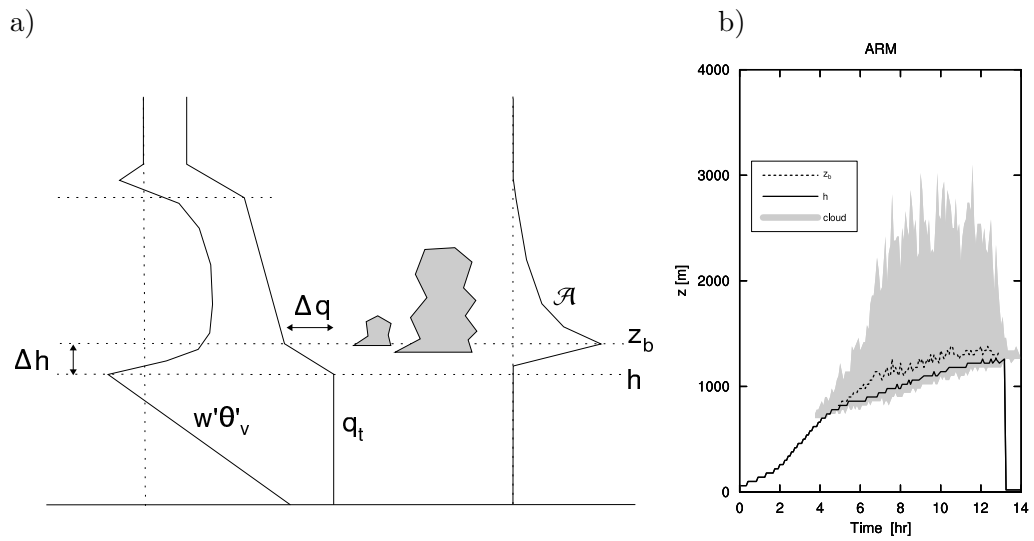


Figure 9. Typical structure of the shallow cumulus topped mixed layer, with a) the profiles of the buoyancy flux $w'\theta'_v$, total specific humidity and cloud core fraction \mathcal{A} . The symbols are defined in the text. b) Time-series of h and z_b for the ARM case. The cloud layer is shaded (grey).

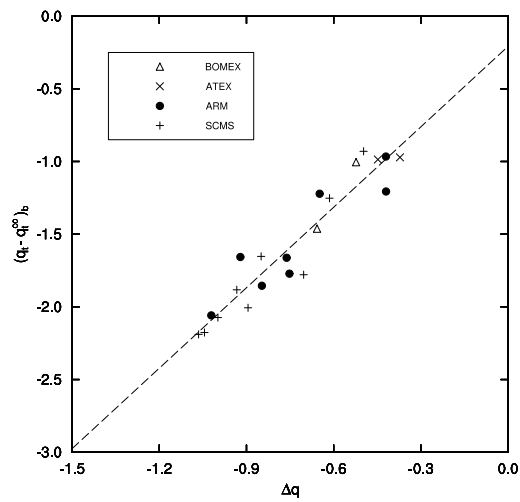


Figure 10. The difference between mean state total specific humidity $\overline{q_t}$ and that of the cloud core q_t^{co} at z_b plotted against the jump in total specific humidity $\overline{q_t}$ between mixed layer top h and cloud base z_b . The points are hourly averages from all cases. The dashed lines represent the least-squares linear fit.

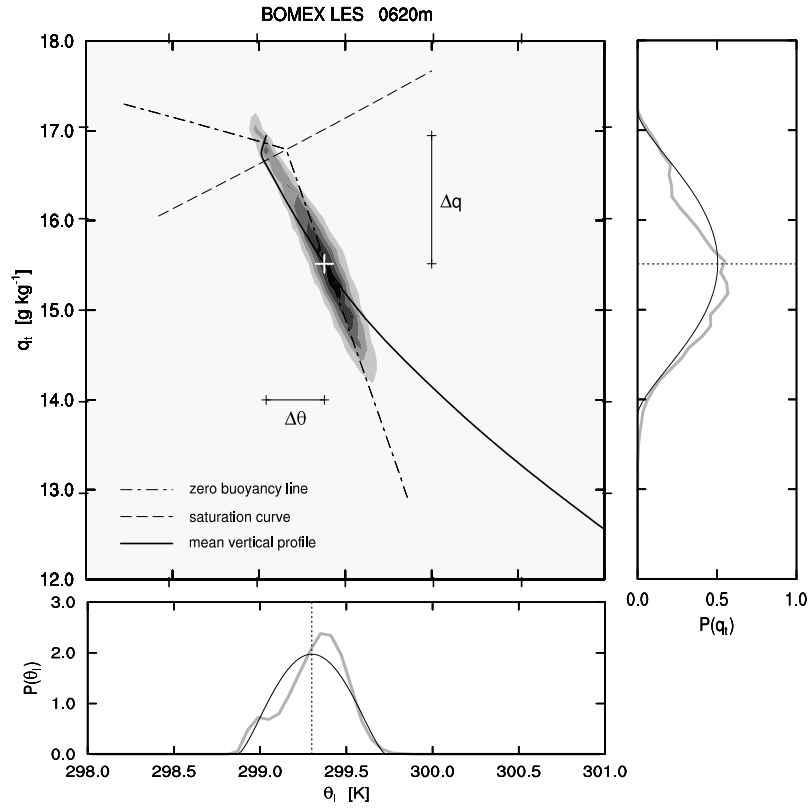


Figure 11. The joint PDF of q_t and θ_t at BOMEX cloud base ($z_b = 620\text{m}$) as obtained from LES. The complete mean vertical profile is also shown (solid), of which the values at z_b are indicated by the cross. The saturation curve and the zero buoyancy line at this particular level are also shown. q_{sat} is the point where the joint PDF intersects the saturation curve, and q_{zb} corresponds to its intersection point with the moist part of the zero buoyancy line. The transition layer jumps Δq and $\Delta\theta_t$ are also shown. The two side panels show the PDF $P(x)$, as in the distribution function $\int P(x)dx = 1$. The solid black lines are the PDFs of the Beta function with $p = r = 2.2$.

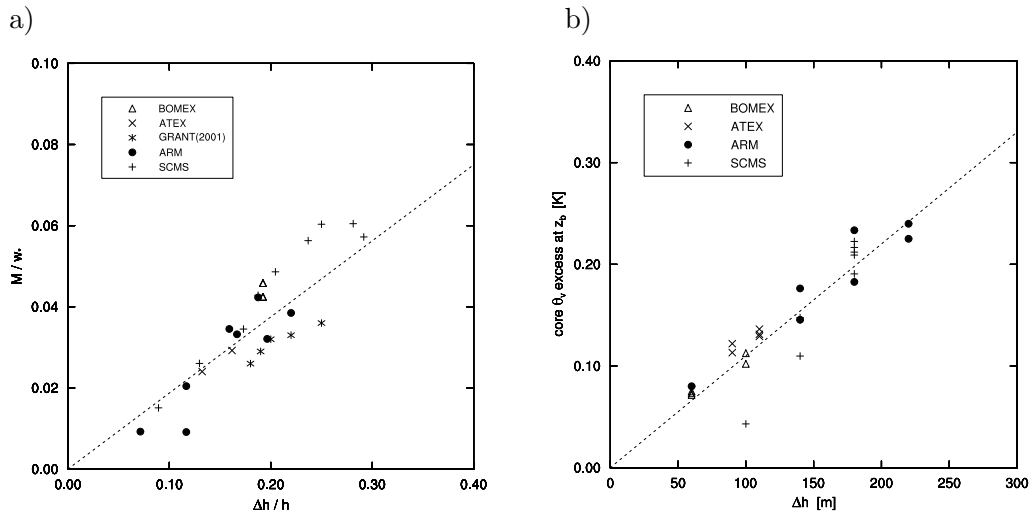


Figure 12. Properties of cumulus cloud base in LES as a function of various parameters. a) Scatter plot of $\Delta z/h$ versus M/w_* . The points are hourly averages from all cases. The results of Grant (2001) are included as well. The dotted line represents the least squares fit of (16), giving $p = 2.2$. b) The depth of the cloud base transition layer Δz versus the θ_v excess of the cloud core over the mean state at z_b . The dotted line represents the least-squares linear fit.

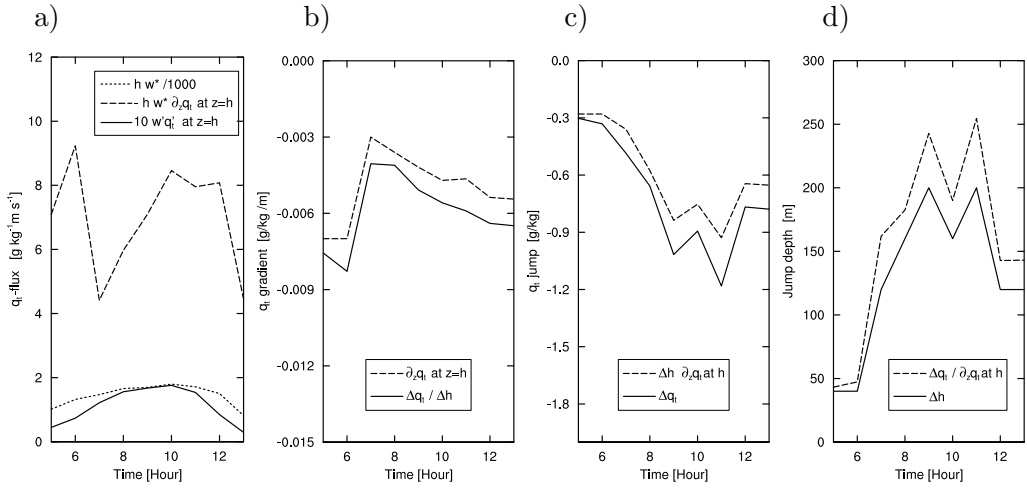


Figure 13. a) Evaluation of the validity of equality (18) in LES during the ARM case. All parameters in the equation are diagnosed individually. Some terms are multiplied by a factor ($10\overline{w'q'_t}$) or constant ($hw_*/1000$) for purpose of display. b) Comparison of the bulk gradient of q_t over the transition layer to the local gradient at $z = h$. c) Transition layer jump of q_t . d) Transition layer depth. In c) and d) the dashed line indicates the value obtained using the local gradient at $z = h$.

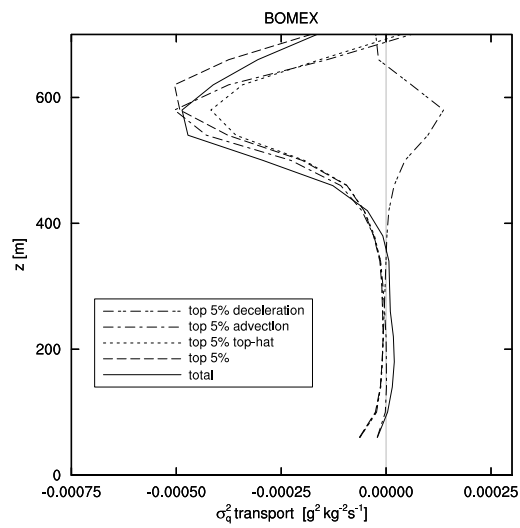


Figure 14. Various terms of decomposition (A.1)-(A.2) of humidity variance transport for the BOMEX case, as sampled in LES. The strongest updraft fraction is defined as the top 5% of the PDF of vertical velocity. Included are the grid-box mean variance transport (solid), the contribution by this top 5% (dashed), the associated top-hat approach (dotted), and the decomposition of the latter into an advection part (dash-dotted) and a deceleration part (dash-double dotted).